Elastic deformations in hexagonal phases studied by small-angle X-ray diffraction and simulations†

**Šárka Perutková,[a] Matej Daniel,[b] Michael Rappolt,[c] Georg Pabst,[c]
Gregor Dolinar,[d] Veronika Kralj-Iglič[e] and Aleš Iglič*[a]**

Received 14th July 2010, Accepted 13th September 2010
DOI: 10.1039/c0cp01187h

In this study we present experimental and theoretical results which concern the deviations from circularity of the pivotal plane in the inverse hexagonal phases (H_{II}) of phospholipid self-assemblies. Due to packing constraints, the cross-section of the polar/apolar interface deviates from a circle, which we studied in minute detail by analysing small-angle X-ray diffraction data of dioleoyl-phosphatidylethanolamine (DOPE) and stearoyl-oleoyl-phosphatidylethanolamine (SOPE), respectively. On this structural basis, Monte Carlo (MC) simulated annealing variations of the free energy were carried out, both on the formation of the H_{II}-phase and on the particular shape of the cross-section in the H_{II}-phase. The equilibrium of the H_{II}-phase pivotal plane contour and the corresponding values of the mean intrinsic curvature, H_m, and the hydrocarbon chain stiffness, τ, were determined from MC calculations. The results of these calculations were tested by solving the corresponding system of non-linear differential equations derived using variational calculus. Here our main aim is to predict the range of possible values of H_m and τ. Comparing the measured structural data with predictions from MC calculations including lipid anisotropy, and accounting for the elastic deformations of the pivotal plane allowed us to determine a relationship between the bending deformation and stretching of hydrocarbon chains.

1. Introduction

Phosphatidylethanolamines (PEs) containing self assemblies have been extensively studied using various methodical approaches.[1,2] The biological relevance of PEs concerns to a large extent their role in forming non-planar membranes in nature.[3,4] For instance, they may promote high local membrane curvature, which is crucial for membrane vesiculation processes.[5,6] Also, non-bilayer forming lipids play a key role in the transient and/or local formation of non-bilayer structures. The different steps of membrane fusion or inter-bilayer tight junctions are believed to host intermediate non-planar structures.[7–10] Last, but not least, (PEs) are indispensable in providing a lipid matrix with special properties, tuning its flexibility and altering its lateral pressure profile,[11] and hence assures the proper function of integral membrane proteins, even in changing environmental conditions.[12–14]

Apart from the relevance of non-bilayer forming lipids in biomembrane processes such as membrane fusion and exocytosis,[15] there is also direct evidence for the formation of non-bilayer structures. For instance, stable domains of the inverted hexagonal phase (H_{II}-phase) have been identified as paracrystalline inclusions in the disk membranes of retinal rod outer segments.[16,17]

Moreover, the H_{II}-phase of biomimetic model systems has been intensively studied in order to characterize the geometric and energetic properties involved.[18–21] For this purpose, most commonly the bending modulus and intrinsic (spontaneous) radii of different lipid/water systems were evaluated. Note that due to the simple geometry of the H_{II}-phase, a clear relationship between the intrinsic shape of the lipid molecules and the given packing frustration is also at hand.[22–24] PEs in the H_{II}-phase were recently also studied by various molecular dynamics simulations.[25–30]

Fig. 1 shows schematically the geometry of the H_{II}-phase which consists of long lipidic monolayer cylinders with radii of a few nanometres arranged in a hexagonal lattice. The phospholipid headgroups are in contact with the water, while the hydrocarbon chains are oriented outwards. Recently it was pointed out by Mareš *et al.*[21] that the concept of the anisotropic shape of lipid molecules may better explain the $L_\alpha - H_{II}$ phase transition and the stability of the H_{II}-phase at higher temperatures rather than the concept of isotropic lipid shapes. A similar idea was also expressed earlier,[31] but not applied to any model calculations. Hence the model of wedge-like shaped phospholipid molecules was favoured over that of inverted cone-like ones[20,21] and the corresponding deviatoric energy term averaging the rotational states of the anisotropic

---

[a] *Laboratory of Biophysics, Faculty of Electrical Engineering, University of Ljubljana, Tržaška 25, SI-1000 Ljubljana, Slovenia. E-mail: ales.iglic@fe.uni-lj.si; Fax: +368 1 476 88 50; Tel: +368 1476 82 35*
[b] *Laboratory of Biomechanics, Faculty of Mechanical Engineering, Czech Technical University in Prague, Technicka 4, CZ-166 07, Prague 6, Czech Republic*
[c] *Institute of Biophysics and Nanosystems Research, Austrian Academy of Sciences, Schmiedlstr. 6, A-8042 Graz, Austria*
[d] *Laboratory of Applied Mathematics, Faculty of Electrical Engineering, University of Ljubljana, Tržaška 25, SI-1000 Ljubljana, Slovenia*
[e] *Laboratory of Clinical Biophysics, Faculty of Medicine, University of Ljubljana, Lipičeva 2, SI-1000 Ljubljana, Slovenia*

† This article was submitted as part of a special collection on scattering methods applied to soft matter, marking the 65th birthday of Professor Otto Glatter.

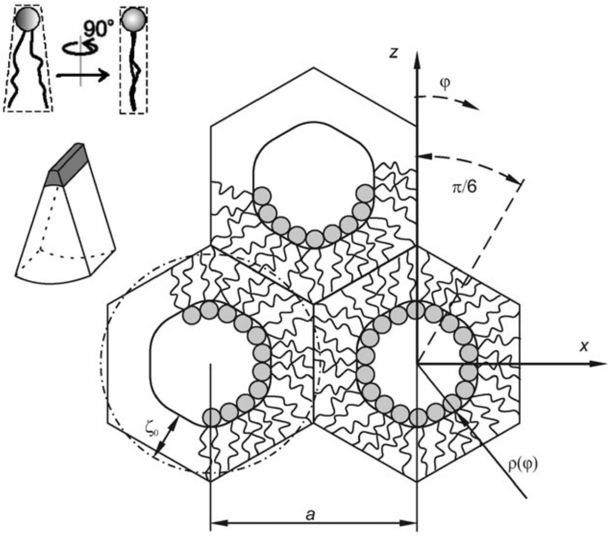

Fig. 1 Cross-section of the H_{II}-phase showing the following geometric parameters: radius vector of the pivotal plane, ρ, unit cell parameter, a, equilibrium length of the hydrocarbon chain, ζ_0, and polar angle, φ. Upper-left corner: model of anisotropic wedge-like shaped phospholipids, where one intrinsic principal curvature is zero and the second is highly negative.

compartments was considered.[32] As in the case of the principal curvatures of the membrane, the anisotropy of the lipid molecules is described by the two principal intrinsic curvatures C_{1m} and C_{2m}.

It is important to note that commonly models of the H_{II}-phase assume isotropic molecule shapes,[33–36] and further presuppose the polar/apolar interface to be perfectly circular, a simplification that was also applied in our latest model calculations.[21,37] In the present work we further generalized our H_{II}-phase model, now also allowing for deviations of the pivotal plane from a circular cross-section, where the pivotal plane is the plane on which the area per lipid molecule is not changed upon applying a bending moment.[34,38] Indeed in reality the cross-section is not purely circular, but appears to be hexagon-like with smoothed edges as was shown in experiments[39,40] and investigated in theories[35,41] and simulations.[25] Although the approximation of circular geometry is more than sufficient for the robust free energy determination of the H_{II}-phase, allowing for deviations from a circular cross-section yields a more accurate evaluation of the membrane material parameters. However, for this it is necessary that the theoretical predictions are cross-checked against highly resolved electron-density maps as given, for instance, for di-oleoyl-phosphatidylethanolamine (DOPE).[39] In the next section two examples of the H_{II}-phase are presented in full structural detail. Our refined model and the theoretical approaches are described in section 3. We note, that the presented theory accounts also for the anisotropy of the molecular shape of the membrane constituents, and thus may be considered an extension of the Helfrich formalism. Finally, the results are presented and also discussed in comparison to literature results, which were derived instead from the classical Helfrich ansatz[42,43] for the free energy of the H_{II}-phase.

2. Materials and Methods

2.1 Sample preparation and X-ray measurements

The preparation of multilamellar vesicles (MLVs) was described in detail in ref. 20. Briefly, 1-stearoyl-2-oleoyl-*sn*-phosphatidylethanolamine (SOPE) was purchased from Avanti Polar Lipids, Inc., Alabaster, AL, USA (purity > 99%) and used without further purification. For the preparation of MLVs, 25 wt% of lipid was dispersed in glass distilled water (HPLC grade, Sigma-Aldrich, Steinheim, Germany). To ensure complete hydration, the lipid dispersions were shock frozen in liquid nitrogen, thereafter thawed for 15 min reaching a final temperature of 50 °C (~19 °C above the main transition), and finally vigorously vortexed for several minutes. This procedure was repeated 10 times.

At 68 °C the static small-angle X-ray diffraction (SAXS) pattern was recorded at the Austrian SAXS beamline at ELETTRA, Trieste.[44,45] The 1D position sensitive detector[46] covered the corresponding s-range ($s = 2\sin(\theta/\lambda)$) of interest from about 1/200 $Å^{-1}$ to 1/12 $Å^{-1}$. The angular calibration of the detector set-up was performed with silver-behenate (d-spacing 58.38 Å[47]). Further sample handling was the same as in ref. 20.

2.2 X-Ray diffraction data analysis

2D electron density maps of the H_{II}-phase were derived from the SAXS pattern using standard procedures (for details see ref. 19). After the raw data had been corrected for detector efficiency, and the background scattering both from water and the sample cell had been subtracted, all Bragg peaks were fitted by Lorentzian distributions. The fittings were carried out with the Origin 5.0 software package (Microcal Software). Next, the intensities were corrected for their multiplicity, *i.e.*, the intensities of the (2,1), (3,1), (3,2) and (4,1) peak were divided by 2. Thereafter, a Lorentz correction was applied to all powder diffraction images by multiplying the peak intensity (peak area) by its corresponding wave vector s^2 (for discussion of the Lorentz correction on powder samples see Warren[48]). Finally, the square-root of the corrected peak intensity determined the form factor $\mathscr{F}$ of each respective reflection. The electron density contrast was calculated by Fourier synthesis

$$\tilde{\rho}(\vec{r}) = \sum_{h,k \neq (0,0)}^{h,k\,\max} \alpha_{h,k} \cdot \mathscr{F}_{h,k} \cdot cos(2\pi \vec{s}_{h,k} \vec{r}), \qquad (1)$$

where $\mathscr{F}(h,k)$ is the amplitude of the peak at the position $\vec{s}_{h,k}$, where h and k are Miller indices and $\alpha_{h,k}$ is its corresponding phase. For centrosymmetric structures, as in this study, the phases for each diffraction order is either +1 or −1. In the inverse hexagonal phase the (1,0), (1,1), (2,0), (2,1), (3,0), (2,2), (3,1), (3,2) and (4,1) reflections were recorded. The best phasing for the H_{II}-phase (+ − − + + + + − −) was taken from ref. 18, where seven different diacyl phosphatidylethanolamines were studied. Note that we checked only the value of $\alpha_{2,1}$, since it has been reported for DOPE that it changes its sign at very high temperatures.[39] Nevertheless, choosing the phase of the (2,1) reflection to negative resulted in too low an electron density for the water region and an unusually strong radial fluctuation of the water core radius.

2.3 Evaluating the pivotal plane cross-section

The cross-section of the pivotal plane was determined from the electron density map (Fig. 2) using Matlab® 7.5. First the phosphate group position with the highest intensity was detected and consequently the pivotal plane position was evaluated. By taking into account that the head-group extension in the radial direction in the hexagonal phase is about 1.1 nm,[39] then the steric lipid/water interface position can be estimated as $R_{\text{phosph}} - 0.55$ nm and the polar/apolar interface position $R_{\text{pivot}} \sim R_{\text{phosph}} + 0.55$ nm, which for DOPE is in very good agreement with the experimentally determined position of the pivotal plane.[49] Nevertheless, the contour lines at R_{phosph} and $R_{\text{phosph}} + 0.55$ nm (determined at $\phi = 0°$) are not perfectly equidistant. Thus the evaluated pivotal plane position varies in the range of ±0.05 nm. The averaged deviations ($\Delta_{\text{phosp}} = (R_{\text{phospMax}} - R_{\text{phospMin}})/R_{\text{phospMax}}$) are $\Delta_{\text{phospSOPE}} = 1.4\%$ and $\Delta_{\text{phospDOPE}} = 2.3\%$ on the phosphate group radius, where R_{phospMin} and R_{phospMax} are the maximum and minimum radii of the phosphate group position.

3. Theory

3.1 Monolayer free energy

The lipid monolayers in the H_{II}-phase have a strong anisotropic curvature therefore the average orientational ordering of the lipids cannot be neglected. The free energy of a lipid monolayer has been derived[32,50] starting from the energy of a single molecule and using the methods of statistical physics. The local bending energy of the lipid monolayer[42] was derived; however, the contribution of the deviatoric bending to the H_{II}-phase was included[32,37] as an additional contribution due to the average orientational ordering of the phospholipids. The whole monolayer free energy is supposed to be:

$$F = F_b + F_v \tag{2}$$

where F_b is the monolayer bending energy comprising of the anisotropy of lipids:[21]

$$F_b = \int_A \frac{n_0 \xi}{2}\left((H - H_m)^2 + D^2 + D_m^2\right) dA - n_0 kT \int_A \ln\left(2\cosh\left(\frac{\xi \tilde{\vartheta} D_m D}{kT}\right)\right) dA \tag{3}$$

Here $H = (C_1 + C_2)/2$ is the local mean curvature of the monolayer, $D = |C_1 - C_2|/2$ is the local curvature deviator, $H_m = (C_{1m} + C_{2m})/2$ is the intrinsic mean curvature, $D_m = |C_{1m} - C_{2m}|/2$ is the intrinsic curvature deviator (for details see ref. 21 and 37), n_0 is the area density of the lipid molecules, ξ is a constant describing the strength of the interaction between a single lipid molecule and the surrounding membrane continuum which is connected to the monolayer bending modulus ($\xi = 2k_c n_0^{-1}$). $\tilde{\vartheta}$ is a constant describing the direct interaction between lipid molecules,[32] k is the Boltzmann constant, T is temperature and dA is the area element of the monolayer surface. We have shown[37,51] that if we take into account the isotropic model of a phospholipid molecule (very small values of curvature deviators D and D_m), eqn (3) for monolayer bending energy turns into the classical Helfrich ansatz.[42,43]

The second contribution F_v is the stretching energy of the lipid chains:[21]

$$F_v = \tau n_0 \int_A (\zeta - \zeta_0)^2 dA. \tag{4}$$

where ζ is the length of the lipid molecule, ζ_0 is the reference length of the molecule and τ is the stretching modulus of the lipid molecule. Considering the H_{II}-phase geometry (Fig. 1), the length of the hydrocarbon chain may be expressed as:

$$\zeta = \frac{a}{2\cos\varphi} - \rho(\varphi) = \sqrt{x^2 + z^2}\left(\frac{a}{2z} - 1\right), \tag{5}$$

where a is the unit cell parameter. The hydrocarbon chain length is described here in both polar and Cartesian coordinates respectively, see Fig. 3, for use in two different methods of calculation. In the following sections we present two different approaches for finding the equilibrium configuration which is determined by the minimum of the membrane free energy F, eqn (2), with constraints relevant to the given case. The deviations from circularity of the pivotal plane cross-section were taken into account in both approaches.

The aim of our calculations was to obtain the equilibrium contour of the pivotal cross-section represented by the unit cell parameter, a, and the polar, $\rho(\varphi)$, or Cartesian, $z(x)$, coordinates for the different membrane parameters H_m and τ with the

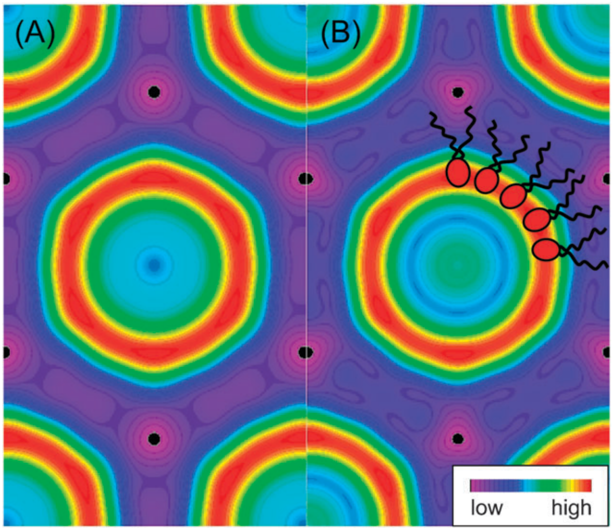

Fig. 2 Electron density maps of (A) DOPE at 20 °C and (B) SOPE at 68 °C with measured lattice spacings (unit cell parameter), a, of 7.58 and 7.42 nm, respectively. The position of the lipid head-groups are coded in red, the water core region in light blue and the hydrocarbon chain regions are highlighted in violet to black. The electron density map of DOPE was recalculated from amplitudes given in ref. 39, while for SOPE the derived amplitudes $F(1,0) = +1.000$, $F(1,1) = -1.070$, $F(2,0) = -0.780$, $F(2,1) = +0.270$, $F(3,0) = +0.330$, $F(2,2) = +0.320$, $F(3,1) = +0.260$, $F(4,0) = +0.009$, $F(3,2) = -0.160$, $F(4,1) = -0.180$ were used for the construction of the density map.

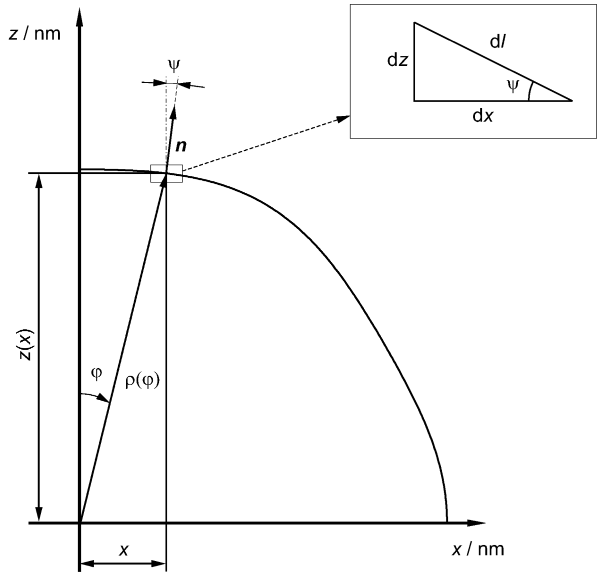

Fig. 3 Illustration of parametrization of the pivotal plane cross-section. The contour is described by Cartesian $z(x)$ and polar $\rho(\varphi)$ coordinates. ψ is the angle between the vertical and normal (**n**) in each point.

Table 1 Values of the optimal (relaxed) length ζ_0 and area per lipid molecule at the pivotal plane $a_0 = n_0^{-1}$ obtained from experiment[39]

	SOPE (68 °C)	DOPE (20 °C)
ζ_0/nm	1.33	1.20
n_0^{-1}/nm^2	5.84	5.97

constants $k_c = 11\ kT$.[52] The values of ζ_0 and n_0^{-1} are given in Table 1 for both phospholipids. The mean and the Gaussian curvatures are $2H = (\partial^2 z/\partial x^2)/(1+(\partial z/\partial x)^2)^{3/2}$ and $C_1C_2 = 0$, respectively. Using the definition of the arc length l and the angle ψ leads to expression: $2H = 2D = \mathrm{d}\psi/\mathrm{d}l$ (see Fig. 3). For the sake of simplicity, we considered the anisotropic shape of the lipids at higher temperatures as wedge-like, having $C_{2\mathrm{m}} = 0$ and $C_{1\mathrm{m}} < 0$ which yields $H_\mathrm{m} = D_\mathrm{m} = C_{1\mathrm{m}}/2$, (Fig. 4c). Because of the hexagonal symmetry it is sufficient to determine the equilibrium contour shape for only one twelfth of the pivotal plane cross-section.

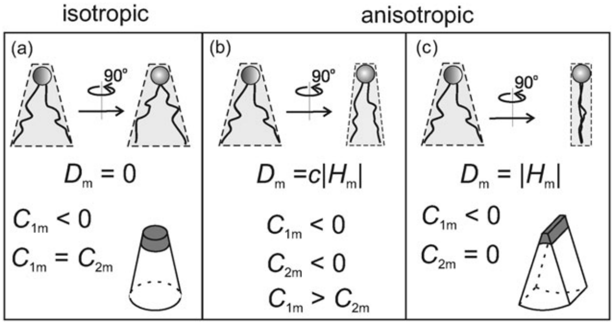

Fig. 4 The difference between isotropic and anisotropic phospholipids: (a) inverted cone-like shape, isotropic; (b) inverted wedge-shape lipid with lower anisotropy; (c) inverted wedge-shape lipid with highest anisotropy.

3.2 Euler–Lagrange equation

In the minimization procedure, the monolayer pivotal surface of the single inverted lipid cylinder in the $\mathrm{H_{II}}$-phase is described by the Cartesian coordinate $z = z(x, y)$. We assume that lipid monolayer cylinders are perfectly straight and thus only the z–x plane was considered and coordinate $z = z(x)$, *i.e.* we assume cylindrical symmetry (see Fig. 3).

The contour coordinates, the length of the lipid chains, the area, the area element and the membrane free energy are written in dimensionless forms. Normalizing the length by an arbitrary z_0 (in our case we set $z_0 = 1$ nm) gives dimensionless curvatures $h = z_0H$, $d = z_0D$, $h_\mathrm{m} = z_0H_\mathrm{m}$, $d_\mathrm{m} = z_0D_\mathrm{m}$, and dimensionless $x/z_0 \to x$, $z/z_0 \to z$, $a/z_0 \to a$, $\zeta_0/z_0 \to \zeta_0$), arc length $l/z_0 \to l$. The area element is $\mathrm{d}A = \mathrm{d}l\,\mathrm{d}y$, further normalized to $\mathrm{d}yz_0$. The energy F is normalized to $n_0\xi\mathrm{d}y/2z_0$,

$$\begin{aligned} f = f_b + f_v = \int (h-h_m)^2\mathrm{d}l + \int (d^2+d_m^2)\mathrm{d}l \\ -\kappa\int \ln(2\cosh(2\tilde{\vartheta}d_m d))\mathrm{d}l \\ +\tilde{\tau}\int ((x^2+z^2)^{1/2}(a/(2z)-1)-\xi_0)^2\mathrm{d}l, \end{aligned} \tag{6}$$

where

$$\kappa = 1/\vartheta = \frac{2kTz_0^2}{\xi},\ \tilde{\tau} = \frac{2\tau z_0^4}{\xi}. \tag{7}$$

To minimize the membrane free energy F a functional

$$\begin{aligned} L = \left(\frac{1}{2}\frac{\mathrm{d}\psi}{\mathrm{d}l} - h_\mathrm{m}\right)^2 + \frac{1}{4}\left(\frac{\mathrm{d}\psi}{\mathrm{d}l}\right)^2 \\ -\kappa\ln\left(2\cosh\left(\tilde{\vartheta}d_\mathrm{m}\frac{\mathrm{d}\psi}{\mathrm{d}l}\right)\right) \\ -\lambda\left(\cos\psi - \frac{\mathrm{d}x}{\mathrm{d}l}\right) - \nu\left(\sin\psi - \frac{\mathrm{d}z}{\mathrm{d}l}\right) \\ +\tilde{\tau}((x^2+z^2)^{1/2}(a/(2z)-1)-\zeta_0)^2 \end{aligned} \tag{8}$$

was constructed, where λ and ν are Lagrange multipliers preserving the boundary conditions. Eqn (8) is minimized by solving a system of Euler–Lagrange equations

$$\frac{\partial L}{\partial \psi} - \frac{\mathrm{d}}{\mathrm{d}l}\left(\frac{\partial L}{\partial \psi_l}\right) = 0, \tag{9}$$

$$\frac{\partial L}{\partial x} - \frac{\mathrm{d}}{\mathrm{d}l}\left(\frac{\partial L}{\partial x_l}\right) = 0, \tag{10}$$

$$\frac{\partial L}{\partial z} - \frac{\mathrm{d}}{\mathrm{d}l}\left(\frac{\partial L}{\partial z_l}\right) = 0, \tag{11}$$

where $\psi_l = \mathrm{d}\psi/\mathrm{d}l$, $x_l = \mathrm{d}x/\mathrm{d}l$ and $z_l = \mathrm{d}z/\mathrm{d}l$. By introducing the variable

$$Y = \frac{\mathrm{d}\psi}{\mathrm{d}l}, \tag{12}$$

the system of eqn (9)–(11) yields

$$\frac{\mathrm{d}Y}{\mathrm{d}l} = (\lambda \sin\psi - \nu\cos\psi)\left(1 - \frac{\kappa\tilde{\vartheta}^2 d_m^2}{\cosh^2(\tilde{\vartheta} d_m Y)}\right)^{-1} \tag{13}$$

$$\frac{\mathrm{d}\lambda}{\mathrm{d}l} = \frac{2\tilde{\tau}x(a/(2z)-1)}{(x^2+z^2)^{1/2}}((x^2+z^2)^{1/2}(a/(2z)-1)-\zeta_0) \tag{14}$$

$$\frac{\mathrm{d}\nu}{\mathrm{d}l} = 2\tilde{\tau}((x^2+z^2)^{1/2}(a/(2z)-1)-\zeta_0) \times \left(\frac{z(a/(2z)-1)}{(x^2+z^2)^{1/2}} - \frac{a(x^2+z^2)^{1/2}}{2z^2}\right) \tag{15}$$

The above system of eqn (13)–(15) was solved numerically by the Mathematica® program to yield the equilibrium contour map of the pivotal plane. The results of these calculations were used to test the accuracy of the MC method described in the next section.

3.3 MC simulated annealing method

Eqn (2) was minimized numerically using the MC simulated annealing method.[53] The contour of the pivotal plane was described by the polar coordinates of the radius vector ρ and the polar angle, $\varphi_i = [0,\pi/6]$, $i = 1,..,N$ which divided a twelfth of the contour line into N points (see Fig. 3). The starting contour for the MC method was the equilibrium geometry where deviations from circularity were not taken into account (computed as described in Mareš *et al.*[21]). The boundary conditions were $\psi = 0$ and $\psi = \pi/6$. In the MC computations ρ_1, ψ_i and a were changed slightly in each step and the energy of the contour was evaluated with respect to the Metropolis criterion, while according to the cooling schedule the temperature parameter was decreased after each step until it reached zero.[53] The radius vector length ρ_i was calculated by using the expression:

$$\rho_{i+1} = \frac{\rho_i(\cos\varphi_i + \sin\varphi_i \mathrm{tg}\psi_i)}{(\cos\varphi_{i+1} + \sin\varphi_{i+1}\mathrm{tg}\psi_i)}. \tag{16}$$

which can be easily derived from Fig. 3.

4. Results

Firstly, the dependence of the mean radius $r_{\mathrm{mean}} = (r_{\mathrm{max}} + r_{\mathrm{min}})/2$ and the deviations from circularity $\Delta = (r_{\mathrm{max}} - r_{\mathrm{min}})/r_{\mathrm{max}}$ were computed as functions of the mean intrinsic curvature H_{m} for different values of the chain stiffness τ in order to quantify the effect of τ on the phospholipid packing during temperature increase. Here $r_{\mathrm{max}} = \max(\rho(\varphi))$ and $r_{\mathrm{min}} = \min(\rho(\varphi))$ are the maximal and minimal radii of the contour, respectively. The temperature dependence of the intrinsic lipid shape in the model is quantitatively simulated by the linear temperature dependence of H_{m} and D_{m}. As already mentioned above, in this work the wedge shape model of a phospholipid was adopted, *i.e.* the wedge angle increases linearly with the temperature.[20,21] It can be seen in Fig. 5a that the higher τ is, the lower the mean radius of the cylinders is. Also the effect of τ on the transition point can be seen (marked by arrows). The simulations show that for higher values of τ, the L_α–H_{II}

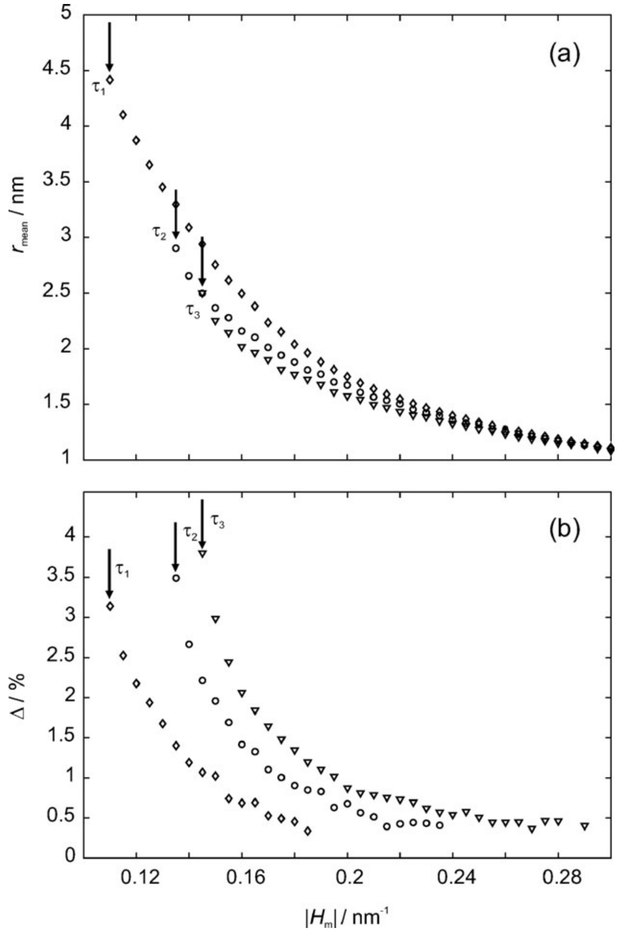

Fig. 5 (a) Mean radius $r_{\mathrm{mean}} = (r_{\mathrm{max}} + r_{\mathrm{min}})/2$ and (b) deviations from circularity $\Delta = (r_{\mathrm{max}} - r_{\mathrm{min}})/r_{\mathrm{max}}$ dependent on $|\boldsymbol{H}_{\mathbf{m}}|$ for different values of hydrocarbon chain stiffness. $\tau_1 = 1.9\ kT\ \mathrm{nm}^{-2}$ (diamonds), $\tau_2 = 9.5\ kT\ \mathrm{nm}^{-2}$ (spheres), $\tau_3 = 19\ kT\ \mathrm{nm}^{-2}$ (triangles). Arrows mark the transition points for each value of τ.

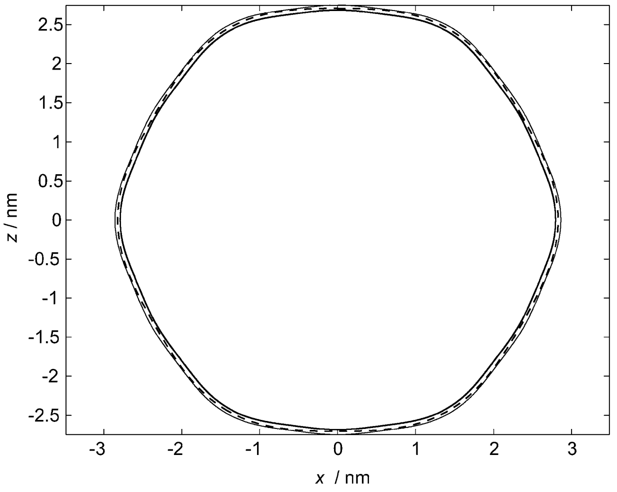

Fig. 6 The best agreement of the experimentally obtained pivotal plane cross-section of DOPE and theoretical predictions. The parameters are $H_{\mathrm{m}} = 0.14\ \mathrm{nm}^{-1}$, $\tau = 14.95\ kT\ \mathrm{nm}^{-2}$.

transition point occurs at higher mean intrinsic curvatures, $|H_m|$, which practically means at higher temperatures (Fig. 5a). On the other hand, the deviations from circularity are higher for τ, (Fig. 5b). The deviations decrease with temperature and above a certain value of $|H_m|$ they become negligible and the shape of the pivotal plane cross-section is circular.

The good agreement of the H_{II}-phase pivotal plane cross-section contour shape between experiments and theoretical predictions for both DOPE and SOPE phospholipids can be seen in Fig. 6 and 7, respectively. Good agreement for the pivotal plane cross-section contour can be achieved for several combinations of H_m and τ. Hence we plotted all the possible solutions (Fig. 8). The range of possible pairs of parameters is restricted to a rather small region in the H_m–τ plane. To reproduce a realistic non-circular shape of the pivotal plane (cp. Fig. 2), τ should not drop below 2 kT nm^2, otherwise even at the low temperatures the shape is too circular ($\Delta < 0.5\%$). The upper limit of possible values for τ is restricted by the magnitude of the realistic mean radii, which become too small for higher τ values. The values of the mean intrinsic curvature H_m are also restricted by the mean radius, namely for higher values of $|H_m|$ the mean radius is too small to match the experimental contour.

To study the dependence of the intrinsic membrane parameters on the temperature, the results were compared with experimental data from Turner and Gruner[39] and the match between possible values of H_m and T was performed with respect to the match of the maximal and minimal radii and the unit cell parameter (Fig. 9). This gives us a qualitative evaluation of the membrane parameters and their dependence on temperature. In Fig. 9 we used $\tau = 9.5\ kT\ \text{nm}^{-2}$ which resulted in $H_m = (0.135–0.159)\ \text{nm}^{-1}$, corresponding to possible values of the intrinsic radius in the range

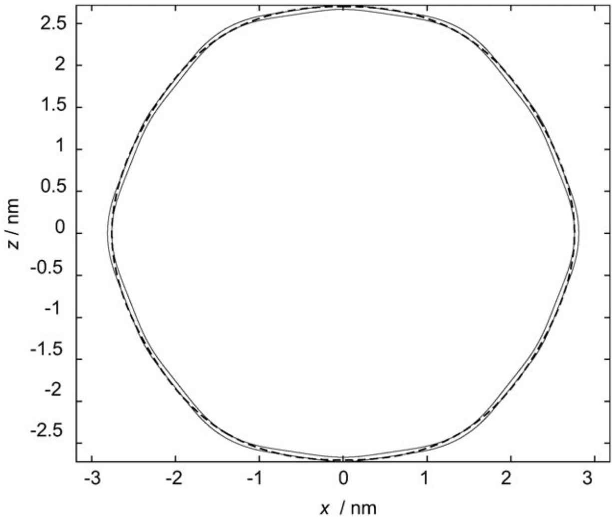

Fig. 7 The best agreement of the experimentally obtained pivotal plane cross-section of SOPE and theoretical predictions. The parameters are $H_m = 0.15\ \text{nm}^{-1}$, $\tau = 1.9\ kT\ \text{nm}^{-2}$.

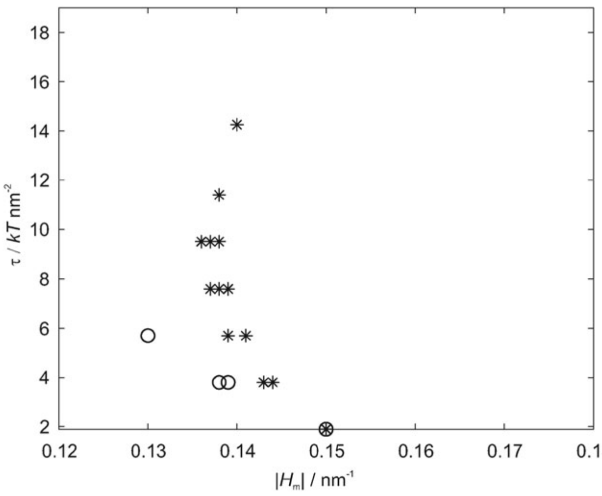

Fig. 8 A plot of $|\boldsymbol{H}_m|$ and τ pairs which are in accordance with experimental data from the electron density maps. SOPE–circles, DOPE–stars.

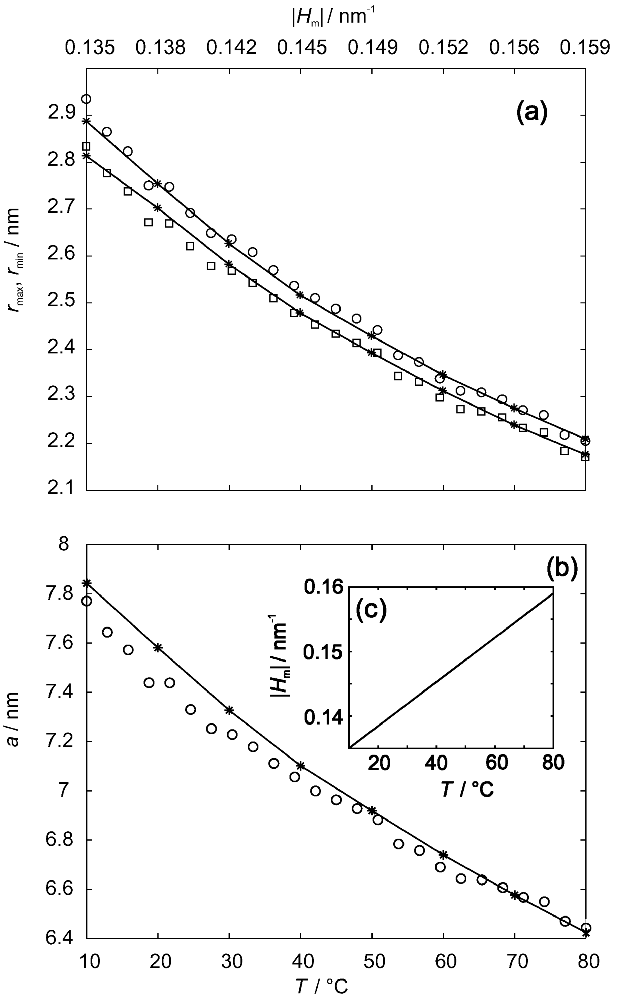

Fig. 9 (a) Maximal and minimal radii of the pivotal plane and (b) unit cell parameter as a function of temperature (experimental results) and mean intrinsic curvature $|\boldsymbol{H}_m|$ (computational prediction). Comparison between experimental results[39] dependent on temperature (line with stars) and theoretical predictions dependent on mean intrinsic curvature $|\boldsymbol{H}_m|$ (circles and squares) is shown. In order to achieve a good agreement between experiment and theory a linear dependence between $|\boldsymbol{H}_m|$ and temperature was assumed, see inset panel (c). Parameters used: DOPE (see Table 1), $\tau = 9.5\ kT\ \text{nm}^{-2}$.

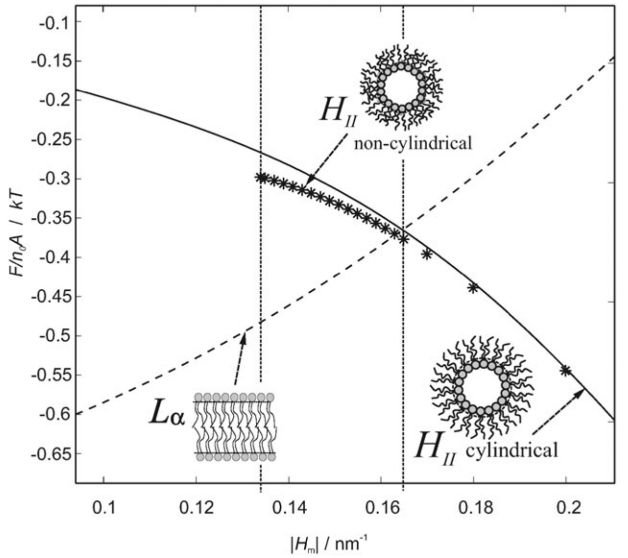

Fig. 10 Free energy per molecule in kT units as a function of the mean intrinsic curvature $|\boldsymbol{H}_{\mathbf{m}}|$. Comparison is shown between the lamellar phase energy (dotted line) and the H_{II}-phase energy for a circular cross-section (full line), as well as for an imperfectly circular cross-section (stars). The two dotted lines indicate the range of theoretical L_α–H_m phase coexistence.

r_m = 3.70 – 3.14 nm. If we take into account the linear dependence of the intrinsic radius $r_m = 0.5|H_m|^{-1}$ on the temperature, we obtain a constant coefficient of 0.008 nm °C^{-1}. This value is constant for different chain stiffnesses.

In Fig. 10 the membrane free energy is plotted as a function of the mean intrinsic curvature $|H_m|$. It is interesting to compare the energy dependences of the H_{II}-phase with circular as well as non-circular (distorted) geometry and the membrane free energy of the lamellar phase for comparison. The energy of the lamellar phase was computed from eqn (3) assuming planar geometry by using the values $H = D = 0$ which means considering only the first non-deviatoric term of the equation. Here a value of chain stiffness $\tau = 9.5\,kT\,\mathrm{nm}^{-2}$ was chosen. It is obvious that taking into account deviations from circularity slightly lowers the membrane free energy with respect to the case of a purely circular geometry. The decrease is more pronounced for higher deviations from circularity. The range of theoretical coexistence of both phases was predicted to be between $|H_m| = (0.134 - 0.165)$, as seen in Fig. 10.

5. Discussion and conclusions

It is important to note that our estimated values of $|H_m|$ should be compared with other literature values with due care. The values of the spontaneous curvature of the membrane monolayer obtained from osmotic pressure and gravimetric measurements[22,38,52,54] are based on the Helfrich theory[42] of an isotropic elasticity model (Fig. 4a). Moreover, we point out that our computations consider the most anisotropic case of the intrinsic lipid shape by setting $|H_m| = D_m$, which means that the second principal intrinsic curvature $C_{2m} = 0$ (Fig. 4c). In reality the most probable value of curvature deviator $|D_m|$ should be smaller and lie somewhere between the two extreme values of 0 and $|H_m|$ (Fig. 4b). This means a general relationship between the mean intrinsic curvature and the curvature deviator $D_m = c|H_m|$ with $C_{2m} = C_{1m}(1 - c)/(1 + c)$, where c reflects the rate of anisotropy, should be applied in future simulations (see Fig. 4). Our predicted linear coefficient of the intrinsic radius temperature dependance (0.008 nm °C^{-1}) is approximately twice as small as the published value of 0.015 nm °C^{-1}.[34] This discrepancy can again be explained by the fact that a direct comparison of $|H_m|$ from isotropic and anisotropic models is not possible. However, factor 2 gives some hint of the possible rate of lipid molecule anisotropy.

It was already shown by Mareš *et al.*[21] that higher mean intrinsic curvatures $|H_m|$ and higher chain stiffnesses, τ, promote a decrease in the pivotal plane cross-section radius and thus promote the transition from a lamellar to an inverted hexagonal phase. In the present work, the deviation from circularity of the pivotal plane cross-section (Δ) was also studied experimentally and theoretically. The predicted dependence of the pivotal plane cross-section on the model parameters H_m and τ can be explained by competition between the bending (F_b) and interstitial (F_v) energies. It can be concluded that when the hydrocarbon chains are very stiff the membrane must bend towards the hexagon corners in order to help to fill the voids. Thus the pivotal plane contour deviates more from a circle as shown in Fig. 5. On the other hand, when the stiffness of the hydrocarbon chain is lower, the chains can easily stretch themselves and in this way fill the voids. As a consequence the H_{II}-phase lipid monolayer does not need to be elastically deformed as much as before.

Acknowledgements

This work was supported by the bilateral Slovenian–Austrian and Austrian–Slovenian grants BI-AT/07-08-022 and WTZ SI17-2009, respectively, bilateral Slovenian–Czech grant BI-CZ/07-08-006 and by the grants MSM6840770012, J3-2120 and P2-0232. The authors are grateful to Dr S. Engelskirchen, Dr C. Kulkarni and P. Earis for inviting us to contribute our paper to the special issue dedicated to the 65th birthday of outstanding researcher and inspiring teacher Prof. Otto Glatter.

References

1 P. Lipowsky and E. Sackmann, *Structure and Dynamics of Membranes. From Cells to Vesicles. Vol. A & B*, Elsevier, 1995.
2 I. N. Serdyuk, N. R. Zaccai and J. Zaccai, *Methods in Molecular Biophysics. Structure, Dynamics, Function*, Cambridge University Press, New York, 2007, pp. 1102.
3 J. M. Seddon, J. Robins, T. Gulik-Krzywicki and H. Delacroix, *Phys. Chem. Chem. Phys.*, 2000, **2**, 4485–4493.
4 T. Kaasgaard and C. J. Drummond, *Phys. Chem. Chem. Phys.*, 2006, **8**, 4957–4975.
5 H. Hägerstrand and A. Iglič, *Mol. Membr. Biol.*, 2006, **23**, 277–288.
6 V. Kralj-Iglič, A. Iglič, H. Hägerstrand and P. Peterlin, *Phys. Rev. E: Stat. Phys., Plasmas, Fluids, Relat. Interdiscip. Top.*, 2000, **61**, 4230–4234.
7 S. Hui, T. Stewart, L. Boni and P. L. Yeagle, *Science*, 1981, **212**, 921–923.
8 D. Siegel, *Biophys. J.*, 1999, **76**, 291–313.
9 D. Siegel and M. Kozlov, *Biophys. J.*, 2004, **87**, 366–374.

10 Y. Kozlovsky and M. M. Kozlov, *Biophys. J.*, 2002, **82**, 882–895.
11 H. Jerabek, G. Pabst, M. Rappolt and T. Stockner, *J. Am. Chem. Soc.*, 2010, **132**, 7990–7997.
12 B. de Kruijff, *Curr. Opin. Chem. Biol.*, 1997, **1**, 564–569.
13 S. M. Gruner, *Proc. Natl. Acad. Sci. U. S. A.*, 1985, **82**, 3665–3669.
14 J. Zimmerberg and M. M. Kozlov, *Nat. Rev. Mol. Cell Biol.*, 2006, **7**, 9–19.
15 R. Jahn, T. Lang and T. C. Sdhof, *Cell*, 2003, **112**, 519–533.
16 J. Corless and M. Costello, *Exp. Eye Res.*, 1981, **32**, 217–228.
17 S. M. Gruner, K. J. Rothschild and N. A. Clark, *Biophys. J.*, 1982, **39**, 241–251.
18 P. E. Harper, D. A. Mannock, R. N. Lewis, R. N. McElhaney and S. M. Gruner, *Biophys. J.*, 2001, **81**, 2693–2706.
19 M. Rappolt, A. Hickel, F. Bringezu and K. Lohner, *Biophys. J.*, 2003, **84**, 3111–3122.
20 M. Rappolt, A. Hodzic, B. Sartori, M. Ollivon and P. Laggner, *Chem. Phys. Lipids*, 2008, **154**, 46–55.
21 T. Mareš, M. Daniel, Š. Perutková, A. Perne, G. Dolinar, A. Iglič, M. Rappolt and V. Kralj-Iglič, *J. Phys. Chem. B*, 2008, **112**, 16575–16584.
22 M. M. Kozlov, *Methods Mol. Biol.*, 2007, **400**, 355–366.
23 M. A. Churchward, T. Rogasevskaia, D. M. Brandman, H. Khosravani, P. Nava, J. K. Atkinson and J. R. Coorssen, *Biophys. J.*, 2008, **94**, 3976–3986.
24 N. Fuller, C. R. Benatti and R. P. Rand, *Biophys. J.*, 2003, **85**, 1667–1674.
25 S.-J. Marrink and A. E. Mark, *Biophys. J.*, 2004, **87**, 3894–3900.
26 S.-J. Marrink and D. P. Tieleman, *Biophys. J.*, 2002, **83**, 2386–2392.
27 V. Knecht, A. E. Mark and S.-J. Marrink, *J. Am. Chem. Soc.*, 2006, **128**, 2030–2034.
28 E. R. May, D. I. Kopelevich and A. Narang, *Biophys. J.*, 2008, **94**, 878–890.
29 F. Suits, M. C. Pitman and S. E. Feller, *J. Chem. Phys.*, 2005, **122**, 244714.
30 M. C. Pitman, F. Suits, K. Gawrisch and S. E. Feller, *J. Chem. Phys.*, 2005, **122**, 244715.
31 R. H. Templer, *Curr. Opin. Colloid Interface Sci.*, 1998, **3**, 255–263.
32 V. Kralj-Iglič, B. Babnik, D. R. Gauger, S. May and A. Iglič, *J. Stat. Phys.*, 2006, **125**, 723–752.
33 R. H. Templer, J. Seddon, P. M. Duesing, R. Winter and J. Erbes, *J. Phys. Chem. B*, 1998, **102**, 7262–7271.
34 M. M. KozIov, S. Leikin and R. P. Rand, *Biophys. J.*, 1994, **67**, 1603–1611.
35 V. S. Malinin and B. R. Lentz, *Biophys. J.*, 2004, **86**, 3324–3328.
36 G. L. Kirk, S. M. Gruner and D. L. Stein, *Biochemistry*, 1984, **23**, 1093–1102.
37 Š. Perutková, M. Daniel, G. Dolinar, M. Rappolt, V. Kralj-Iglič and A. Iglič, in *Advances in Planar Lipid Bilayers and Liposomes*, ed. A. L. Liu and H. Tien, Elsevier, 2009, vol. 9, ch. Stability of the Inverted Hexagonal Phase, pp. 237–278.
38 S. Leikin, M. M. Kozlov, N. L. Fuller and R. P. Rand, *Biophys. J.*, 1996, **71**, 2623–2632.
39 D. C. Turner and S. M. Gruner, *Biochemistry*, 1992, **31**, 1340–1355.
40 J. M. Seddon, *Biochim. Biophys. Acta*, 1990, **1031**, 1–69.
41 M. Hamm and M. Kozlov, *Eur. Phys. J. B*, 1998, **6**, 519–528.
42 W. Helfrich, *Z. Naturforsch.*, 1973, **28c**, 693–703.
43 H. J. Deuling and W. Helfrich, *J. Phys.*, 1976, **37**, 1335–1345.
44 H. Amenitsch, M. Rappolt, M. Kriechbaum, H. Mio, P. Laggner and S. Bernstorff, *J. Synchrotron Radiat.*, 1998, **5**, 506–508.
45 S. Bernstorff, H. Amenitsch and P. Laggner, *J. Synchrotron Radiat.*, 1998, **5**, 1215–1221.
46 A. M. Petrascu, M. H. J. Koch and A. Gabriel, *J. Macromol. Sci., Part B: Phys.*, 1998, **37**, 463–483.
47 T. C. Huang, H. Toraya, T. N. Blanton and Y. Wu, *J. Appl. Crystallogr.*, 1993, **26**, 180–184.
48 B. E. Warren, *X-Ray Diffraction*, Addison-Wesley, Reading, 1969.
49 R. P. Rand and N. L. Fuller, *Biophys. J.*, 1994, **66**, 2127–2138.
50 J. Fournier, *Phys. Rev. Lett.*, 1996, **76**, 4436–4439.
51 M. Fonarič, K. Bohinc, D. R. Gauger, A. Iglič, V. Kralj-Iglič and S. May, *J. Chem. Inf. Model.*, 2005, **45**, 1652–1661.
52 Z. Chen and R. P. Rand, *Biophys. J.*, 1997, **73**, 267–276.
53 S. Kirkpatrick, C. D. Gelatt and M. P. Vecchi, *Science*, 1983, **220**, 671–680.
54 R. M. Epand, N. Fuller and R. P. Rand, *Biophys. J.*, 1996, **71**, 1806–1810.